EES Catalysis

PAPER

View Article Online
View Journal | View Issue

Cite this: *EES Catal.*, 2024, 2, 1126

Received 30th April 2024,
Accepted 11th June 2024

DOI: 10.1039/d4ey00094c

rsc.li/eescatalysis

Bridging the structural gap of supported vanadium oxides for oxidative dehydrogenation of propane with carbon dioxide†

Li Wang,[ab] Heng-Bo Zhang,[a] Rongrong Hu,[a] Han-Qing Ge,[a] Yong-Hong Song,[a] Guo-Qing Yang,*[a] Yuefeng Li,[b] Zhao-Tie Liu[a] and Zhong-Wen Liu*[a]

As an extensively used industrial catalyst for oxidation reactions, supported vanadium oxide (VO_x) is a promising candidate for oxidative dehydrogenation of propane with carbon dioxide (CO_2-ODP). Although the structure of VO_x is found to be a key factor in determining the catalytic activity and stability of supported VO_x for CO_2-ODP, the essential reason still remains elusive at the molecular level. To shed some light on this fundamental issue, VO_x/(−)SiO_2 catalysts with narrow distributions of V loading while well-defined structures of VO_x species, *i.e.*, monomeric VO_x, less polymeric VO_x, highly polymeric VO_x and V_2O_5 crystallites, were purposely synthesized by appropriate methods, including one-pot hydrothermal synthesis, incipient wetness impregnation and physical grinding. We found that the catalytic activity and stability of VO_x species decrease in the order of monomeric VO_x > less polymeric VO_x > highly polymeric VO_x > crystalline V_2O_5, which coincides with the ability for the re-oxidation of the correspondingly reduced VO_x species by CO_2. As a result of the most facile re-oxidation of the reduced monomeric VO_x species by CO_2, a well matched redox cycle of V^{5+}/V^{4+} oxides during CO_2-ODP can be maintained with increasing the time on stream, leading to an improved stability of the catalyst with more monomeric VO_x. These mechanistic findings on the redox properties of VO_x with different structures can be guidelines for developing a high-performance VO_x-based catalyst for CO_2-ODP.

Broader context

Although the oxidative dehydrogenation of propane with carbon dioxide (CO_2-ODP) is a sustainable route for the efficient production of propene in tandem with CO_2 reduction to CO, the rational design of high-performance catalysts for this green process is challenged by limited understanding of the nature of active sites and the reaction mechanism. Supported vanadium oxides (VO_x) are promising for CO_2-ODP considering their low price, environmental sustainability, and competitive catalytic performance, however the essential reason of VO_x structural effects on the catalytic performance is still ambiguous from a mechanistic aspect. In present work, SiO_2-supported VO_x catalysts with narrow distributions of V loading while well-defined structures of VO_x species, *i.e.*, monomeric VO_x, less polymeric VO_x, highly polymeric VO_x and V_2O_5 crystallites, were on-purpose synthesized. In addition to sophisticated catalytic tests for CO_2-ODP, complementary characterization techniques were applied for deriving structural and mechanistic insights into catalyst functioning. We established that the catalytic activity and stability of different VO_x species coincide well with the ability for the re-oxidation of correspondingly reduced VO_x by CO_2. These findings are important guidelines for purposeful development of efficient supported VO_x catalysts for CO_2-ODP.

1. Introduction

Among the currently available methods, the production of propene from propane through either the direct dehydrogenation or the oxidative dehydrogenation reaction is the most competitively favorable route.[1,2] However, only the direct propane dehydrogenation (PDH) technologies are commercialized on large scales, which characterize low propene productivity and high energy consumption.[2,3] To overcome these shortcomings, the oxidative dehydrogenation of propane using carbon dioxide as a soft oxidant (CO_2-ODP) has attracted much attention.[3,4] In comparison with PDH, CO_2-ODP can promote the equilibrium conversion of propane by removing the produced hydrogen *via* CO_2 reduction. Moreover, CO_2-ODP favors a higher propene selectivity than that by using O_2 as an oxidant due to the soft oxidizing

---

[a] *Key Laboratory of Syngas Conversion of Shaanxi Province, School of Chemistry & Chemical Engineering, Shaanxi Normal University, Xi'an 710119, China. E-mail: gqyang@snnu.edu.cn, zwliu@snnu.edu.cn*

[b] *Kaili Catalyst & New Materials Co., Ltd, Xi'an 710201, China*

† Electronic supplementary information (ESI) available. See DOI: **https://doi.org/10.1039/d4ey00094c**

ability of CO_2. Importantly, the efficient production of two value-added products of propene and CO from propane and the greenhouse gas of CO_2, respectively, turns CO_2-ODP into a charming tandem process from an environmental viewpoint.[4,5] Moreover, although the separation of gaseous species resulting from the introduction of CO_2 remains a significant challenge, the CO_2-ODP product mixtures can be directly used as feeds to produce useful chemicals, such as the oxidative coupling of CO_2 with alkenes to produce acrylic acids and acrylate in a one-step process, which is a more energy-saving and efficient technology than the conventional two-step methodology.[6] As a result of these advantages, a number of catalysts including supported or bulk metal oxides *e.g.*, Cr,[7] V,[8] In,[9] Ga,[10] and Zn,[11] and supported metals, *e.g.*, Pd,[12] and Pt[13,14] have been extensively studied for CO_2-ODP. Among these potential catalysts, supported vanadium oxides (VO_x) are promising for CO_2-ODP considering their low price, environmental sustainability and competitive catalytic performance.[2,15] However, the rational design of a high-performance supported VO_x catalyst is still challenging due to limited understanding of the active and stable nature of VO_x species as well as the reaction mechanism.

Indeed, the apparent turnover frequency (TOF) of the supported VO_x for activating propane during CO_2-ODP has been revealed to be decreased with increasing the polymerization degree of VO_x species.[16,17] A similar conclusion is also valid for the oxidative dehydrogenation of ethylbenzene with CO_2 reaction, in which monomeric VO_x are more active and more stable than polymeric VO_x and crystalline V_2O_5.[18] Although these observations are tentatively correlated with the structural and chemical properties of VO_x species with different structures, the essential reason in the mechanistic aspect, especially the activation of CO_2 and the balance between the activations of C–O bonds in CO_2 and C–H bonds in C_3H_8 molecules, is still ambiguous. In the cases of the reducible metal oxide catalysts, *e.g.*, CrO_x and VO_x, the CO_2-ODP reaction may follow the Mars–van-Krevelen redox mechanism.[8,19] Thus, the redox cycles of the VO_x species participated with CO_2 and propane must proceed quickly in a well-matched manner, which is essential for a high-performance VO_x. Specifically, the active oxygen species in VO_x with a higher oxidation number of +5 is consumed by activating propane molecule to produce propene and water, accompanying the formation of VO_x with a lower oxidation state (+4 and/or +3), which is re-oxidized to be V^{5+} by CO_2 for the simultaneous formation of CO. If the weak oxidizing ability of CO_2 is taken into account, the re-oxidation of V^{4+} and/or V^{3+} to V^{5+} by CO_2 may be a key step in the redox cycle. With these considerations, the catalytic performance of different VO_x species for CO_2-ODP may be closely related to their different abilities for activating and converting CO_2 molecules. However, the detailed mechanistic understandings are still of lacking, and only the partial re-oxidation of the reduced VO_x species by CO_2 is reported.[20,21]

As a common practice, supported VO_x with the structures of monomeric VO_x, less or highly polymeric VO_x and even crystalline V_2O_5 can be achieved by adjusting the V loadings of the catalyst. However, in this case, the V loadings commonly vary in large ranges from about 0.3 wt% to 20 wt%,[22–24] which makes it difficult to unambiguously correlate the catalytic performance of VO_x catalysts with their structures. This can be reflected from different observations for oxidative dehydrogenation of propane with O_2 catalyzed by VO_x/Al_2O_3, *i.e.*, the decreased[25] and constant[26] TOF of propane with increasing the V loadings. On the one hand, the catalyst with a very low V loading makes it difficult to perform the accurately qualitative and quantitative analysis of the characterization and reaction results, thus a lager error may be present. On the other hand, if the loading of V is too high, the intrinsic concentration of the adsorption and activation of feed components and reaction products on per active site of V on the catalyst surface during the reaction, may be affected by the steric constraint effect, leading to an inauthentic conclusion when the reaction results are discussed. Thus, the catalysts with different VO_x structures while narrow V loading distributions are desired for better understanding the essential reason of the VO_x structural effects on the catalytic performance of VO_x for CO_2-ODP.

As a matter of fact, in addition to adjusting V loadings, the catalysts with different VO_x structures can be also obtained by changing the preparation methods.[27,28] To date, the widely reported methods for preparing supported VO_x catalysts are one-step direct synthesis and impregnation method.[29,30] Generally, at a given loading of V, the VO_x species prepared by one-step synthesis shows a higher dispersion than that synthesized by the impregnation method due to the incorporation of VO_x species into the framework of the support.[31] Additionally, supported crystalline V_2O_5 can be obtained by the directly physical grinding method due to the weakened interaction between the VO_x precursor and the support.[32,33]

Based on these understandings, in this work, $VO_x/(-)SiO_2$ catalysts with 4–6 wt% V loadings are purposefully designed and prepared by different methods. As a result, well-defined structures of VO_x species over the catalysts, *i.e.*, monomeric VO_x, less polymeric VO_x, highly polymeric VO_x and crystalline V_2O_5, are achieved as confirmed from the characterization results. More importantly, the structural impacts of different VO_x species on the activations of C–O bonds in CO_2 are rigorously revealed from the results of the pulse experiments, and the balance between the activations of C–O bonds in CO_2 and C–H bonds in C_3H_8 molecules induced from different VO_x species is established together with the reaction and characterization data. These understandings can provide important contributions to the essential reason of the structural impacts of VO_x species on CO_2-ODP, especially the activations of C–O bonds in CO_2 and the balance between the activations of C–O bonds in CO_2 and C–H bonds in C_3H_8 molecules, which are key factors in determining the catalytic activity and stability of the catalysts.

2. Experimental

2.1. Catalyst preparation

The one-pot hydrothermal synthesis[29] was used to prepare the SiO_2-supported VO_x catalyst with a V loading of 4 or 6 wt%. In the detailed procedure, 1.74 g of cetyltrimethyl ammonium bromide (CTAB, ≥99.0%, Guanghua Sci-Tech Co., Ltd, Guangdong, China) and 0.25 g of sodium hydroxide (NaOH, ≥96.0%, Guanghua Sci-Tech Co. Ltd, Guangdong, China) were dissolved into 70 mL of deionized water. The ammonium metavanadate with desired amount (NH_4VO_3, ≥99.0%, Fuchen Chemical Reagent Co. Ltd, Tianjin, China) was dissolved into 25 mL of deionized water at 60 °C. Then, above solutions were completely mixed at 60 °C under magnetic stirring. After 30 min, 9.14 mL of tetraethyl orthosilicate (TEOS, 98.0%, Macklin Biochemical Co. Ltd, Shanghai, China) was slowly dropped into the mixture under magnetic stirring. After 2 h, the obtained mixture was transferred to a Teflon autoclave and crystallized at 120 °C for 2 days. The solids were centrifuged, washed several times by water and ethanol until the pH value of filtrate is neutral, and then dried at 120 °C for 6 h and calcined in air at 600 °C for 3 h. The obtained catalysts were named as $4VO_x$–SiO_2-H and $6VO_x$–SiO_2-H, respectively, where 4 and 6 are the weight percent of V (wt%), and H represents the hydrothermal synthesis method.

The incipient wetness impregnation method was applied to prepare the SiO_2-supported VO_x catalyst with a V loading of 6 wt%. Before loading VO_x, SiO_2 with a BET surface area of 580 $m^2\ g^{-1}$ and an average pore diameter of 3.0 nm (Fuji Silysia Chemical Ltd, Kasugai Aichi, Japan) was pre-treated in air at 600 °C for 3 h. After impregnating the desired amounts of aqueous solution of NH_4VO_3 assisted by oxalic acid (99.6%, Sinopharm Chemical Reagent Co. Ltd) at a molar ratio of 1/2, the sample was dried at 120 °C for 6 h and then calcined in air at 600 °C for 3 h. The obtained catalyst was named as $6VO_x/SiO_2$-I, where 6 is the V loading (wt%), and I represents the impregnation method.

The SiO_2-supported VO_x catalyst with a V loading of 6 wt% was also prepared by the physical grinding method. The same SiO_2 support (2 g) to that used in the impregnation experiment was directly blended with 0.275 g of NH_4VO_3 powders. After grinding for 30 min in an agate mortar, the sample was dried at 120 °C for 6 h and calcined in air at 600 °C for 3 h, leading to the catalyst of $6VO_x/SiO_2$-P, where 6 is the V loading (wt%), and P represents the physical grinding method.

2.2. Catalyst characterizations

The loading of V over the catalyst was determined by inductively coupled plasma mass spectrometry (ICP-MS, Bruker Dalton-Aurora M90). Before the test, about 10.0 mg of sample was dissolved in a mixed solution of HNO_3 (Sinopharm, 70%) and HF (Sinopharm, ≥30%) at 60 °C for 30 min.

N_2 physical adsorption/desorption isotherms were performed on a Bel-sorp-Max instrument at −196 °C. Before the measurement, each sample was pre-treated at 300 °C under vacuum for 10 h. The Brunauer–Emmett–Teller (BET) equation and Barrett–Joyner–Halenda (BJH) method were employed to calculate specific surface area and pore size distribution (PSD) of the catalysts, respectively.

Powder X-ray diffraction (XRD) patterns were obtained on an X-ray diffractometer equipped with Cu-Kα radiation (Bruker D8 Advance, 40 kV, 40 mA). The sample was scanned from 2θ value of 10° to 80° with a speed of 0.2 s per step.

Raman spectra of the fresh catalysts in the range of 200–1200 cm^{-1} were obtained by a confocal microprobe laser Raman spectrometer (HORIBA Jobin Yvon) equipped with the laser of 325 and 532 nm, respectively. The peak at 520.7 cm^{-1} of a silica standard was used to calibrate the obtained spectra. The sample was loaded into an *in situ* cell (Harrick, HVCDR2) and dehydrated at 400 °C under dried Ar (40 mL min^{-1}) for 40 min. After cooling to ambient temperature in an Ar flow, Raman spectra were collected. The Raman spectra of the spent catalysts for CO_2-ODP were directly recorded in the range of 1100–1700 cm^{-1} with the laser of 532 nm at ambient environment.

In situ UV-Vis diffuse reflectance spectra (UV-Vis DRS) were acquired on a PerkinElmer Lambda 950 spectrophotometer equipped with an *in situ* cell (Harrick, HVCDR2). The sample was previously diluted with $BaSO_4$ (≥99.0%, Macklin Biochemical Co. Ltd, Shanghai, China), and then pre-treated at 400 °C under Ar (30 mL min^{-1}) for 40 min. After cooling to room temperature, the spectra were recorded in the range of 200–800 nm by using $BaSO_4$ as the background. The absorption edge energy (E_g) was determined by the intercept of the straight line, which is fitted through the low energy rise in $[F(R_\infty)\cdot h\nu]^2$ *versus* the photon energy plot ($h\nu$), where $F(R_\infty)$ is the Kubelka–Munk function.

Temperature-programmed reduction with H_2 (H_2-TPR) tests were carried out using an Autochem 2920 instrument (Micromeritics, USA) equipped with a thermal conductivity detector (TCD). 100.0 mg of sample was pre-treated at 400 °C for 30 min in an Ar flow (30 mL min^{-1}). After cooling to 50 °C, the sample was heated from 50 to 800 °C with a rate of 10 °C min^{-1} in a 10 vol% H_2/Ar flow (30 mL min^{-1}). H_2 consumption was monitored and determined by a pre-calibrated TCD.

X-ray photoelectron spectroscopy (XPS) measurements were performed on an Axis Ultra spectrometer (KRATOS Analytical Ltd) equipped with an Al-Kα radiation source (1486.6 eV). The C 1s spectrum at 284.6 eV was applied to calibrate the obtained spectra of the samples.

CO_2 pulse experiments were performed on an AutoChem 2950 HP Chemisorption instrument (Micromeritics, USA). 0.25 g of catalyst was pre-reduced by 10 vol% H_2/Ar (30 mL min^{-1}) at 600 °C for 1 h. After purging with Ar (30 mL min^{-1}) for 30 min, pulse of CO_2 (0.5 mL loop) mixed with a flow of Ar (20 mL min^{-1}) passed through the reduced catalyst. The temporal change of CO_2 (m/z = 44) and the product of CO (m/z = 28) were monitored by an HPR QIC20 mass spectrometer (MS, Hiden Analytical, United Kingdom). Because the energy of ion source used in MS is relatively low (electron energy: 18.0 V; emission: 50 μA), the signal of 28 (m/z) from CO_2 is negligible.

Thermo gravimetric and differential scanning calorimetry tests (TG-DSC) for the spent catalysts were carried out on a Q600SDT Thermoanalyzer System (TA Instruments). About 5.0 mg of sample was heated from 30 to 800 °C with a heating ramp of 10 °C min^{-1} in a flow of air (50 mL min^{-1}).

2.3. Catalytic tests

Reaction tests were performed at 0.1 MPa in a quartz fixed-bed reactor (6 mm, i.d.). For each test, 0.25 g of catalyst (40–60 mesh) was loaded into the reactor. Firstly, the sample was pre-treated at 600 °C for 30 min in an Ar flow of 20 mL min^{-1}, and then the gas mixture of Ar/C_3H_8/CO_2 (32 mL min^{-1}) in a molar ratio of 2/3/27 passed through the catalyst, where Ar is an internal standard gas. The products and unconvertible C_3H_8 and CO_2 were analyzed by an online gas chromatograph (GC7920, Peking CEAULIGHT) equipped with TCD (TDX-01 column) and flame ionization detector (FID, Porapak Q column). Conversion of propane and CO_2, and selectivity of different hydrocarbon products (CH_4, C_2H_4, C_2H_6 and C_3H_6) were calculated by eqn (1)–(3), respectively.

Carbon balances for all catalysts during the reaction calculated by eqn (4) were centered at 99.3 ± 0.7% (Fig. S1, ESI†), indicating a very small amount of coke deposits formed on the catalyst surface. Thus, by assuming that the carbon balance is 100%, the selectivity of CO produced from C_3H_8 *via* the reforming of propane with CO_2 reaction (CO_2-RP) was estimated by subtracting the sum of the hydrocarbon products (CH_4 + C_2H_4 + C_2H_6 + C_3H_6) from 100% (eqn (5)) according to ref. 13 and 34.

$$\mathrm{C_3H_8\ conversion} = \frac{[F_{\mathrm{C_3H_8}}]_{\mathrm{inlet}} - [F_{\mathrm{C_3H_8}}]_{\mathrm{outlet}}}{[F_{\mathrm{C_3H_8}}]_{\mathrm{inlet}}} \times 100\% \tag{1}$$

$$\mathrm{CO_2\ conversion} = \frac{[F_{\mathrm{CO_2}}]_{\mathrm{inlet}} - [F_{\mathrm{CO_2}}]_{\mathrm{outlet}}}{[F_{\mathrm{CO_2}}]_{\mathrm{inlet}}} \times 100\% \tag{2}$$

$$\mathrm{Selectivity\ of\ product}\ i = \frac{n_i \times [F_i]_{\mathrm{outlet}}}{3 \times \left([F_{\mathrm{C_3H_8}}]_{\mathrm{inlet}} - [F_{\mathrm{C_3H_8}}]_{\mathrm{outlet}}\right)} \times 100\% \tag{3}$$

$$\mathrm{Carbon\ balance} = \frac{\sum_i n_i \times [F_i]_{\mathrm{outlet}} + 3 \times [F_{\mathrm{C_3H_8}}]_{\mathrm{outlet}} + [F_{\mathrm{CO}}]_{\mathrm{outlet}} + [F_{\mathrm{CO_2}}]_{\mathrm{outlet}}}{3 \times [F_{\mathrm{C_3H_8}}]_{\mathrm{inlet}} + [F_{\mathrm{CO_2}}]_{\mathrm{inlet}}} \times 100\% \tag{4}$$

$$\mathrm{CO\ selectivity} = \left(1 - \sum_i \frac{n_i \times [F_i]_{\mathrm{outlet}}}{3 \times \left([F_{\mathrm{C_3H_8}}]_{\mathrm{inlet}} - [F_{\mathrm{C_3H_8}}]_{\mathrm{outlet}}\right)}\right) \times 100\% \tag{5}$$

where, $F_{C_3H_8}$, F_{CO_2} and F_{CO} is the volumetric flow rate (mL min^{-1}) of C_3H_8, CO_2 and CO, respectively, i stands for the detected hydrocarbon product of CH_4, C_2H_6, C_2H_4 or C_3H_6, and F_i and n_i represent the flow rate and carbon number of the hydrocarbon product, respectively.

Relative deactivation rate (R) calculated by eqn (6) was used to evaluate the stability of catalyst.

$$R = \frac{X_{\mathrm{initial}} - X_{\mathrm{final}}}{X_{\mathrm{initial}}} \times 100\% \tag{6}$$

where X_{initial} and X_{final} is the initial and final conversion of propane or CO_2 at time on stream (TOS) of 8 and 128 min, respectively. High R value means low stability of the catalyst.

To estimate the effects of the internal or external diffusion limitations on the catalytic performance, the Weisz–Prater (C_{WP}) and Mears' criteria (C_{MM}) were used for $6VO_x$–SiO_2-H with the highest propane conversion according to ref. 35–37. The detailed calculations are given in Section 12 in the ESI.† The calculated C_{WP} of 1.54×10^{-3} and C_{MM} of 2.82×10^{-3} are significantly lower than those of the critical values of 1 and 0.15, respectively. This suggests that both internal and external diffusion limitations are negligible for the applied reaction conditions.

The propane consumption rate ($r(C_3H_8)$, mmol g^{-1} min^{-1}) was calculated using eqn (7). The apparent TOF(C_3H_8) defined as the number of C_3H_8 molecules converted per V atom per hour over the catalysts was calculated by eqn (8), and the TOF(CO_2) was determined through the same method. The data were determined after a TOS of 5 min at a low propane/CO_2 conversion below 10% by adjusting the amount of the loaded catalyst under the conditions of 600 °C, 0.1 MPa, Ar/C_3H_8/CO_2/He molar ratio = 2/3/3/24, total flow rate = 32 mL min^{-1}.

$$r(\mathrm{C_3H_8}) = \frac{[F_{\mathrm{C_3H_8}}]_{\mathrm{inlet}} - [F_{\mathrm{C_3H_8}}]_{\mathrm{outlet}}}{22\,400 \times m_{\mathrm{cat}}} \tag{7}$$

$$\mathrm{TOF(C_3H_8)} = \frac{r(\mathrm{C_3H_8}) \times 60}{c} \tag{8}$$

where 22 400, m_{cat} and c stand for the molar volume at standard conditions (mL mol^{-1}), catalyst mass (g), and the content of V over the catalyst (mmol g^{-1}), respectively.

3. Results and discussion

3.1. Structural and chemical properties of the catalysts

The amounts of V over the $4VO_x$–SiO_2-H, $6VO_x$–SiO_2-H, $6VO_x$/SiO_2-I and $6VO_x$/SiO_2-P catalysts were determined by ICP-MS. According to the results given in Table 1, the nominal V loading of $4VO_x$–SiO_2-H is exactly the same, to the measured value of 4.0 wt% within the experimental errors. In the cases of the catalysts with 6 wt% V, the measured values (5.7–5.8 wt%) are also very close to the nominal V loadings.

XRD results of the catalysts are shown in Fig. 1a. For $4VO_x$–SiO_2-H and $6VO_x$–SiO_2-H, only a broad peak at about 22.6° corresponding to the SiO_2 support with amorphous nature was detected, suggesting the presence of highly dispersed VO_x species. Contrary to this, additionally weak reflections at 2θ of 20.3°, 26.2° and 31.1° were observed for $6VO_x$/SiO_2-I, which are assigned to (001), (110), and (400) crystal planes of crystalline V_2O_5, respectively.[18,22] In the case of $6VO_x$/SiO_2-P, the more

Table 1 Measured V loading and calculated specific surface area of the catalysts

Catalyst	V loading (wt%)	Surface area (m^2 g^{-1})
$4VO_x$–SiO_2-H	4.0	810
$6VO_x$–SiO_2-H	5.7	809
$6VO_x$/SiO_2-I	5.8	518
$6VO_x$/SiO_2-P	5.8	496

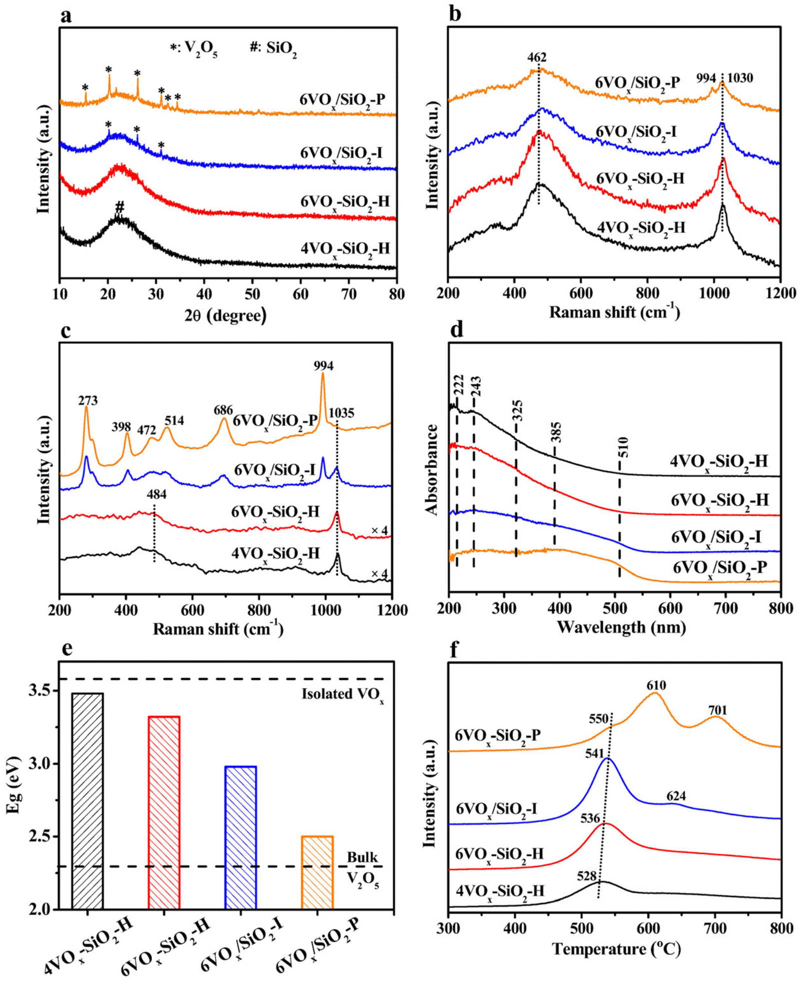

Fig. 1 XRD patterns (a), *in situ* UV (b) and visible (c) Raman spectra, *in situ* UV-vis DRS spectra (d), calculated edge energy (e) and H_2-TPR profiles (f) of the catalysts.

and stronger diffraction peaks assigned to crystalline V_2O_5 were observed. These results indicate that the structures of VO_x over these catalysts are different, even though the V loadings are in a narrow distribution. The $4VO_x$–SiO_2-H and $6VO_x$–SiO_2-H catalysts prepared by one-pot hydrothermal synthesis show a higher dispersion of VO_x.

Textural properties of the catalysts were analyzed by N_2 adsorption–desorption isotherms. As given in Fig. S2a (ESI†), all catalysts exhibited the similar type-IV isotherms with an H1-type hysteresis loop, which are typical characteristics of the capillary condensation of N_2 in mesoporous materials with uniform channels. This can be further reflected from the very narrow PSD peaks at about 3 nm determined by the BJH method (Fig. S2b, ESI†). From the calculated textural parameters summarized in Table 1, the specific surface areas of $4VO_x$–SiO_2-H and $6VO_x$–SiO_2-H were about $\sim$800 $m^2\ g^{-1}$, which are clearly higher than that of $6VO_x/SiO_2$-I and $6VO_x/SiO_2$-P ($\sim$500 $m^2\ g^{-1}$). This commonly leads to a higher dispersion of VO_x, coinciding with the XRD results (Fig. 1a).

To further identify the structure of VO_x species over these catalysts, *in situ* UV and visible Raman were applied under dehydrated conditions. Generally, the former is more sensitive to detect isolated and polymerized VO_x species, while the latter shows a higher sensitivity to crystalline V_2O_5.[22,23,38] As shown in the Fig. 1b, two UV Raman bands at $\sim$460 and 1030 cm^{-1} were clearly observed over $4VO_x$–SiO_2-H and $6VO_x$–SiO_2-H, which can be assigned to V–O–Si and V═O stretching vibrations, respectively.[38–40] However, an additionally weak Raman band at 994 cm^{-1} was detected for $6VO_x/SiO_2$-I and $6VO_x/SiO_2$-P, indicating the presence of crystalline V_2O_5.[22,41] This can be more clearly reflected by the visible Raman spectra as given in Fig. 1c. Only the Raman band at $\sim$1035 cm^{-1} and the weak and broad band at about 484 cm^{-1} assigned to V═O vibration and the SiO_2 support,[38,40] respectively, were observed in the spectra of $4VO_x$–SiO_2-H and $6VO_x$–SiO_2-H. However, the Raman bands at 273, 398, 472, 514, 686, and 994 cm^{-1} assigned to crystalline V_2O_5 were clearly observed in the case of $6VO_x/SiO_2$-I.[40] Furthermore, the intensity of these Raman bonds becomes more pronounced in the spectrum of $6VO_x/SiO_2$-P, accompanying an almost disappearance of V═O vibration at 1035 cm^{-1}. This suggests the formation of dominated crystalline V_2O_5 over $6VO_x/SiO_2$-P.

To estimate the polymerization degree of VO_x over these catalysts, *in situ* UV-Vis DRS experiments were performed under dehydrated condition. As shown in Fig. 1d, a broad absorption band from about 200 to 550 nm was observed in all the spectra of the catalysts because of the ligand-to-metal charge transfer (LMCT) transitions and the d–d transitions of V ions. According to ref. 42 and 43 the coordination and polymerization degree of VO_x species are closely connected with the band position of LMCT transitions. Specifically, the absorption features at 222 and 243 nm can be assigned to strongly and less distorted isolated VO_x in tetrahedral coordination environment, respectively.[31,44] The bands at 325 and 385 nm are generally assigned to oligomeric VO_x species in either tetrahedral or octahedral coordination environment.[37,45] Additionally, the octahedral V_2O_5 crystallites can be observed at $\sim$510 nm.[37,45] For $4VO_x$–SiO_2-H, the strongest bonds at 222 and 243 nm were observed. However, the intensity of these two bonds was decreased over $6VO_x$–SiO_2-H, accompanying the enhanced signals at 325 and 385 nm. This indicates that the $4VO_x$–SiO_2-H catalyst shows the most isolated VO_x species, while more polymeric VO_x was formed over $6VO_x$–SiO_2-H. In the case of $6VO_x/SiO_2$-I, an extremely weak band at 510 nm was observed, indicating the presence of both polymeric VO_x and a small amount of crystalline V_2O_5. As for $6VO_x/SiO_2$-P, the intensity of the band at 510 nm became more pronounced, suggesting the presence of higher amount of crystalline V_2O_5.

Furthermore, the edge energy (E_g) of these catalysts was determined based on the UV-Vis DRS results. As shown in Fig. S3 (ESI†) and 1e, the calculated E_g decreased in the order of $4VO_x$–SiO_2-H (3.48 eV) > $6VO_x$–SiO_2-H (3.32 eV) > $6VO_x/SiO_2$-I (2.90 eV) > $6VO_x/SiO_2$-P (2.50 eV), indicating an increased degree of polymerization or domain size of VO_x.[18,24] Moreover, the E_g for $4VO_x$–SiO_2-H was very close to that for the bulk Na_3VO_4 (3.55 eV) only consisting of isolated VO_x species.[46] Thus, the isolated VO_x species was dominated over $4VO_x$–SiO_2-H. However, in the case of $6VO_x/SiO_2$-P, the E_g was comparable with that of the bulk V_2O_5 (2.33 eV),[46] suggesting the presence of dominated crystalline V_2O_5.

To study the redox property of the VO_x species over the catalysts, H_2-TPR was performed. As shown in Fig. 1f, only a reduction peak at around 530 °C was observed for $4VO_x$–SiO_2-H and $6VO_x$–SiO_2-H, which can be easily assigned to the reduction of highly dispersed VO_x species.[47,48] For $6VO_x/SiO_2$-I, two peaks at 541 and 624 °C were observed. The former originates from the reduction of highly dispersed VO_x species, while the weak peak at 624 °C can be attributed to the reduction of a small amount of microcrystalline V_2O_5.[49] In the case of $6VO_x/SiO_2$-P, three peaks at 550, 610 and 701 °C were present. The shoulder peak at 550 °C can be assigned to the reduction of a small amount of highly dispersed VO_x species, while two sharp peaks at higher temperatures originate from the different stages for the reduction of bulk V_2O_5 from V^{5+} to V^{4+}, and then to V^{3+}.[50] Moreover, the continuously increased peak temperatures in the order of $4VO_x$–SiO_2-H (528 °C) < $6VO_x$–SiO_2-H (536 °C) < $6VO_x/SiO_2$-I (541 and 624 °C) < $6VO_x/SiO_2$-P (550, 610 and 701 °C) indicate an increased difficulty in the reduction of the catalysts with a higher polymerization extent or a larger domain size of VO_x species.[29,49]

As for the oxidation state of V over the fresh catalysts, a symmetric V $2p_{3/2}$ peak with a binding energy of 517.6 eV was observed in all XP spectra of the catalysts (Fig. S4, ESI†), suggesting that V^{5+} is dominated species on the catalysts surface.[18,22] Taking this fact and the total amounts of H_2 consumption during H_2-TPR into account, the average oxidation state (AOS) of V over different catalysts after H_2-TPR was calculated. As given in Table 2, the AOS of V decreased in the order of $4VO_x$–SiO_2-H (+4.06) < $6VO_x$–SiO_2-H (+3.88) < $6VO_x/SiO_2$-I (+3.62) < $6VO_x/SiO_2$-P (+3.35). This indicates that the reduction degree of VO_x species increases with increasing its polymerization degree or domain size, leading to a more favorable reduction of V^{5+} to V^{3+} instead of V^{4+}.[18,22]

Based on these complementary characterizations, the dominated structures of VO_x over the four catalysts are proposed and illustrated in Scheme 1. It can be concluded that (1) monomeric VO_x species is dominantly present over $4VO_x$–SiO_2-H; (2) monomeric and less polymeric VO_x coexist over the $6VO_x$–SiO_2-H catalyst; (3) highly polymeric VO_x and a small amount of crystalline V_2O_5 are present over $6VO_x/SiO_2$-I; and (4) crystalline V_2O_5 is overwhelmingly dominated in the case of $6VO_x/SiO_2$-P.

3.2. Catalytic performance

The initial conversion of propane and CO_2 at a TOS of 8 min over the catalysts for CO_2-ODP is given in Fig. 2a. The propane conversion decreased from 41.0% to 11.9% in the order of $6VO_x$–SiO_2-H > $4VO_x$–SiO_2-H > $6VO_x/SiO_2$-I > $6VO_x/SiO_2$-P. If the CO_2 conversion is compared, the same changing order can be observed. Considering the fact that the V loadings of these catalysts are very close, the results suggest that the structure of VO_x plays an important role in determining the catalytic activity.

As show in Fig. 2b, the initial propene selectivity decreased from 87.3% to 67.7% in the order of $4VO_x$–SiO_2-H > $6VO_x$–

Table 2 Calculated results based on the H_2-TPR and CO_2 pulse experiments of the catalysts

Catalyst	H_2 consumption[a] (μmol $g_{catalyst}^{-1}$)	H/V ratio[a]	AOS of V[a]	Released CO[b] (μmol $g_{catalyst}^{-1}$)	Released CO[b] (mmol g_V^{-1})
$4VO_x$–SiO_2-H	358	0.94	+4.06	270	6.74
$6VO_x$–SiO_2-H	621	1.12	+3.88	353	5.89
$6VO_x/SiO_2$-I	766	1.38	+3.62	225	3.76
$6VO_x/SiO_2$-P	915	1.65	+3.35	36	0.61

[a] Calculated based on the H_2-TPR results as given in Fig. 1f. [b] Cumulative amount of CO formed from the pulse of CO_2 over the reduced catalyst at 600 °C as given in Fig. 4a–d.

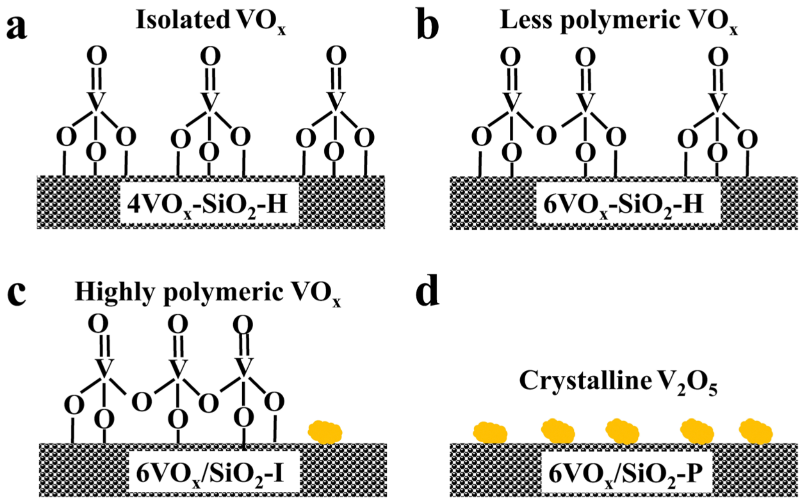

Scheme 1 Illustration of the dominated VO$_x$ species over 4VO$_x$–SiO$_2$-H (a), 6VO$_x$–SiO$_2$-H (b), 6VO$_x$/SiO$_2$-I (c) and 6VO$_x$/SiO$_2$-P (d).

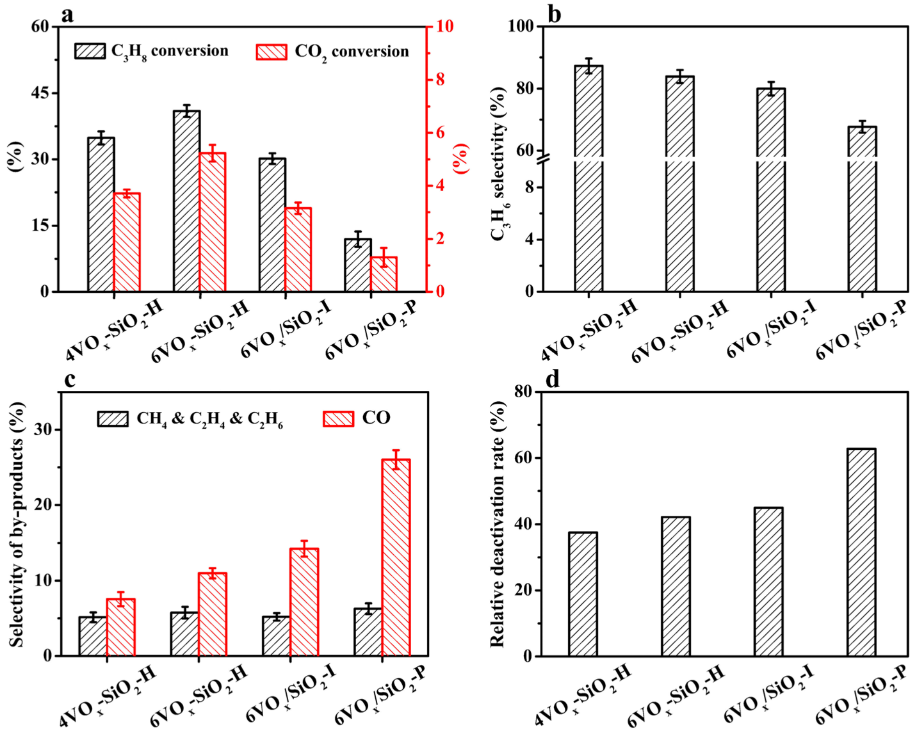

Fig. 2 Initial conversion of C_3H_8 and CO_2 (a), C_3H_6 selectivity (b) and by-products selectivity (c), and the relative deactivation rate (d) over the catalysts for CO_2-ODP under the conditions of 600 °C, 0.1 MPa, Ar/C_3H_8/CO_2 molar ratio = 3/2/27, total flow rate = 32 mL min^{-1}, and GHSV = 7680 mL g^{-1} h^{-1}.

SiO_2-H > 6VO$_x$/SiO$_2$-I ≫ 6VO$_x$/SiO$_2$-P. To understand the main side reactions, the initial selectivity of gaseous by-products was analyzed. As shown in Fig. 2c, CH_4, C_2H_4 and C_2H_6 originating from the cracking and CO produced from the CO_2-RP reaction were detected. For all catalysts, the total selectivity for the by-products of CH_4, C_2H_4 and C_2H_6 was centered at around 5%. However, the selectivity of CO increased from 7.6% to 26.0% in the order of 4VO$_x$–SiO$_2$-H < 6VO$_x$–SiO$_2$-H < 6VO$_x$/SiO$_2$-I ≪ 6VO$_x$/SiO$_2$-P. The change order is inverse to that of the propene selectivity (Fig. 2b), suggesting that the formation of desired propene is strongly affected by the side reaction of CO_2-RP during the reaction. The 4VO$_x$–SiO$_2$-H catalyst with the highest dispersion of VO$_x$ species, *i.e.*, the dominantly monomeric VO$_x$, showed the highest propene selectivity. With increasing the degree of polymerization or domain size of VO$_x$, the amounts of active site over the catalyst which are favorable for CO_2-RP involving the breaking of C–C bond increased, leading to the lowest propene selectivity over the 6VO$_x$/SiO$_2$-P catalyst with dominantly crystalline V_2O_5. A similar result is observed in the chemical looping oxidative dehydrogenation of propane catalyzed by VO_x/TiO_2, suggesting that the highly dispersed VO_x is the main active species for the oxidative dehydrogenation of propane.[51]

In the case of the catalytic stability, an apparently decreased conversion of either propane or CO_2 with increasing TOS was observed for all catalysts (Fig. S5a and b, ESI†). To quantitatively estimate the stability of the catalysts, the relative deactivation rate associated with propane conversion was calculated (R_{propane}, see eqn (6)). As given in Fig. 2d, the stability of the catalysts varied in a lager extent, and R_{propane} increased in the order of $4VO_x$–SiO_2-H < $6VO_x$–SiO_2-H < $6VO_x/SiO_2$-I < $6VO_x/SiO_2$-P. The same change pattern was observed when the relative deactivation rate was calculated based on the CO_2 conversion (R_{CO_2}, Fig. S6, ESI†), resulting in the best stability of the $4VO_x$–SiO_2-H catalyst.

3.3. Structural correlation of VO_x with the catalytic activity

As revealed from the results in Sections 3.1 and 3.2, the catalytic activity of supported VO_x for CO_2-ODP is closely connected with the polymerization extent or domain size of VO_x species. To further confirm this, the apparent TOF(C_3H_8) of the catalysts calculated by eqn (8) were correlated with the E_g values derived from the UV-vis DRS. As shown in Fig. 3, with decreasing the E_g, the TOF(C_3H_8) continuously decreased in the order of $4VO_x$–SiO_2-H > $6VO_x$–SiO_2-H > $6VO_x/SiO_2$-I > $6VO_x/SiO_2$-P, leading to the highest TOF(C_3H_8) of $4VO_x$–SiO_2-H with dominantly monomeric VO_x. In the case of the $4VO_x$–SiO_2-H and $6VO_x$–SiO_2-H catalysts, no crystalline V_2O_5 can be detected, and only two-dimensional VO_x species is present. Moreover, the textural properties of $4VO_x$–SiO_2-H and $6VO_x$–SiO_2-H, *i.e.* the surface area and pore size distributions are almost the same (Table 1 and Fig. S2, ESI†), which commonly leads to the very similar V distributions on the SiO_2 support. Thus, the decreased TOF(C_3H_8) can be ascribed to the increased in the polymerization degree of VO_x.[16,17] However, the crystalline V_2O_5 is formed over the $6VO_x/SiO_2$-I and $6VO_x/SiO_2$-P catalysts, in which not all V atoms can be touched with the reactants during the reaction. Thus, the decreased TOF(C_3H_8) from $6VO_x/SiO_2$-I to $6VO_x/SiO_2$-P is determined by both the increased polymerization degree of VO_x and the formation of more crystalline V_2O_5. These analyses together with the structures of VO_x illustrated in Scheme 1 indicate that the activity of VO_x species for CO_2-ODP decreases in the order of monomeric VO_x > less polymeric VO_x > highly polymeric VO_x > crystalline V_2O_5. If the apparent TOF(CO_2) of the catalyst was calculated and correlated with the E_g (Fig. S7, ESI†), exactly the same change pattern to that of the TOF(C_3H_8) was observed, and the highest value was obtained over $4VO_x$–SiO_2-H, indicating the simultaneous activation of propane and CO_2. Moreover, the TOF(CO_2) of the catalyst is generally lower than its TOF(C_3H_8), which can be attributed to the weak ability for the activation of CO_2 over the supported VO_x species.[52]

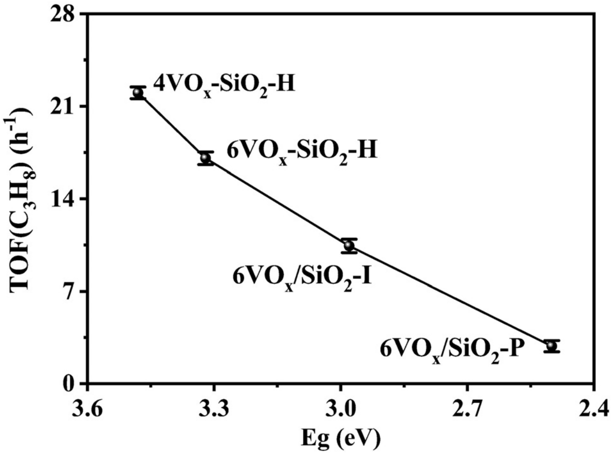

Fig. 3 Relationship between TOF(C_3H_8) and E_g derived from UV-vis DRS of the catalysts.

According to the Mars–van Krevelen redox mechanism for CO_2-ODP catalyzed by supported VO_x catalysts,[8,53] the activated propane molecules abstract the active oxygen from the VO_x species with a high V oxidation state (+5) to produce propene and water. Simultaneously, VO_x at a reduced state is re-oxidized by the activated CO_2 to complete the redox cycle of VO_x with releasing CO. Thus, the re-oxidized ability of V^{3+}/V^{4+} by CO_2 may be crucial in determining the activity of the catalyst, if the facile redox property of supported VO_x at high temperatures and the soft oxidizing ability of CO_2 are taken into account. Following this understanding, the re-oxidized ability of the reduced catalysts by CO_2 was investigated by CO_2 pulse experiments at the reaction temperature of 600 °C. As shown in Fig. 4a–d, when CO_2 (m/z = 44) was pulsed, CO (m/z = 28) was detected over all the catalysts pre-reduced by H_2. Moreover, for pure SiO_2 support prepared by hydrothermal synthesis method, no CO signal (m/z = 28) was detected (Fig. S8, ESI†). These results indicate that the reduced VO_x species can be re-oxidized by CO_2 to replenish the oxygen species consumed by H_2 reduction. Moreover, as shown in Table 2, the amounts of released CO per gram of the catalyst varied in a large range, and decreased from 353 to 36 μmol g_{catalyst}^{-1} in the order of $6VO_x$–SiO_2-H > $4VO_x$–SiO_2-H > $6VO_x/SiO_2$-I > $6VO_x/SiO_2$-P. This indicates that the re-oxidized ability of reduced VO_x species by CO_2 is affected by the structure of VO_x over the parent catalysts. To further confirm this, the amounts of released CO per gram of V over the catalyst were calculated (Table 2), and continuously decreased from 6.74 to 0.61 mmol g_V^{-1} in the order of $4VO_x$–SiO_2-H > $6VO_x$–SiO_2-H > $6VO_x/SiO_2$-I > $6VO_x/SiO_2$-P. Thus, the re-oxidized ability of the reduced catalysts by CO_2 decreases with increasing the polymerization extent or domain size of VO_x over the parent catalysts, and $4VO_x$–SiO_2-H with dominantly monomeric VO_x shows the best ability for the activation of CO_2 to release CO. As for the reason, on the one hand, the H_2-TPR results have demonstrated that the V^{5+} oxide species with a higher polymerization extent or domain size over the parent catalysts was more easily reduced to a lower V oxidation state of V^{3+} rather than V^{4+} (Table 2), which is difficult to be re-oxidized by CO_2 to V^{5+} if the soft oxidizing property of CO_2 was taken into account.[54,55] On the

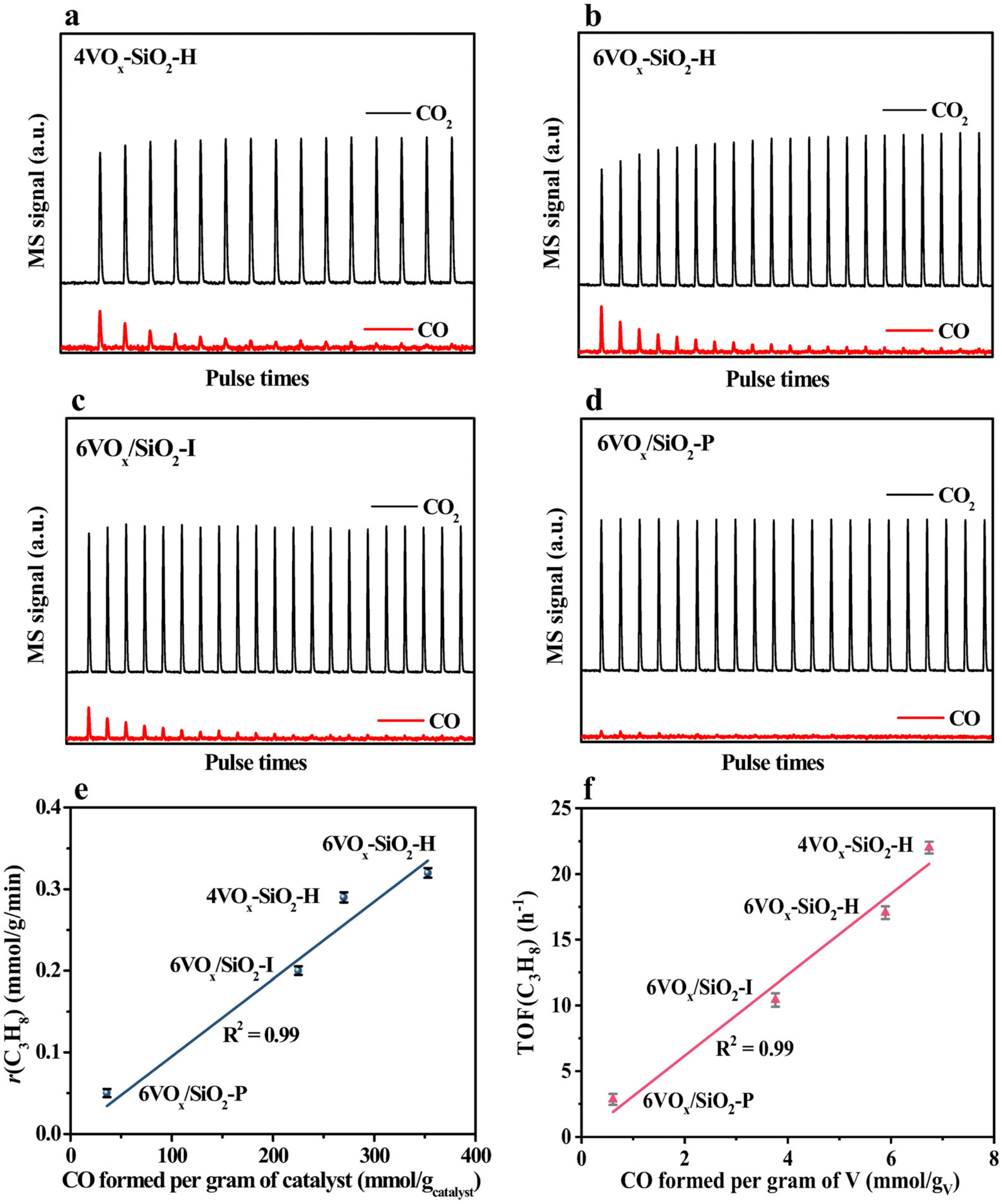

Fig. 4 Transient MS response of the consecutive CO_2 pulses over the pre-reduced catalysts at 600 °C (a)–(d), and correlating the propane consumption rate with the amount of cumulatively released CO per gram of catalyst (e) and the TOF(C_3H_8) with the amount of cumulatively released CO per gram of V (f) during the CO_2 pulse experiments.

other hand, the CO_2 pulse experiments were performed at 600 °C, however the $6VO_x$–SiO_2-P catalyst, which exhibits a reduction peak at a higher temperature of about 700 °C during H_2-TPR, may not be fully reduced at 600 °C. This also led to a lower amount of released CO when CO_2 was pulsed. Moreover, the amount of released CO (270 μmol $g_{catalyst}^{-1}$) during the CO_2 pulse experiments over $4VO_x$–SiO_2-H with the best ability for the activation of CO_2 is still lower than the amount of H_2 consumption (358 μmol $g_{catalyst}^{-1}$) during the H_2-TPR (Table 2). This indicates that the reduced VO_x species cannot be fully re-oxidized by CO_2 owning to the weak oxidizing ability of CO_2.

Based on these understandings, the consumption rate of propane ($r(C_3H_8)$, mmol g^{-1} min^{-1}) was rationally correlated with the amount of formed CO per gram of catalyst (mmol $g_{catalyst}^{-1}$) determined by CO_2 pulse experiments. As shown in Fig. 4e, a directly proportional relationship was obtained, and $r(C_3H_8)$ monotonously increased in the order of $6VO_x/SiO_2$-P < $6VO_x/SiO_2$-I < $4VO_x$–SiO_2-H < $6VO_x$–SiO_2-H with increasing the amount of formed CO. The higher amount of formed CO during the CO_2 pulse experiments means the supplement of more active oxygen species over the reduced catalysts by CO_2 reduction. Thus, this result clearly indicates that the activity of the parent catalyst is determined by the ability in activating CO_2 to replenish the consumed oxygen species of the reduced catalyst, coinciding with the Mars–van-Krevelen redox mechanism. To further understand the relationship between the structure of VO_x and the catalytic activity, the TOF(C_3H_8) was correlated with the amount of formed CO per gram of V. As shown in Fig. 4f, with increasing the amount of released CO per gram of V, the TOF(C_3H_8) increased in the order of $6VO_x/SiO_2$-P < $6VO_x/SiO_2$-I < $6VO_x$–SiO_2-H < $4VO_x$–SiO_2-H. The reduced $4VO_x$–SiO_2-H catalyst with dominantly monomeric VO_x species is the most easily re-oxidized by CO_2, thereby the parent catalyst can well complete the redox cycle of VO_x during CO_2-ODP, resulting in the highest TOF(C_3H_8).

3.4. Insight into the catalytic stability

Generally, the coke deposition on the catalyst surface during the CO_2-ODP reaction is associated with the catalyst deactivation. Thus, the spent catalysts after a TOS of 128 min were analyzed by TG, and the results are given in Fig. S9a–d (ESI†). According to ref. 11 and 16, the weight loss in the temperature range of 25–200 °C is attributed to the removing of adsorbed water, while the weight loss in the temperature range of 200–450 °C can be reasonably assigned to the burning of the deposited coke on catalyst surface. In our case, the coke content of the catalysts determined by the weight loss at 200–450 °C during TG was very low and varied in the range of 0.41 to 0.91% (Table 3). When the coke species was considered, visible Raman was performed for the spent catalysts at ambient environment. As shown in Fig. S10 (ESI†), typical Raman shifts at 1340 and 1600 cm^{-1}, assigning to the disordered (D band) and graphitic carbon (G band),[16,56] respectively, were clearly detected for all the spent catalysts. Generally, the graphitization degree of deposited coke can be estimated by the calculated intensity ratio of the D band to G band (I_D/I_G).[16,56] As given in Table 3, the I_D/I_G was determined as 0.74 ± 0.08 for $4VO_x$–SiO_2-H, $6VO_x$–SiO_2-H and $6VO_x/SiO_2$-I, indicating the similar coke species on the surface of catalysts. Contrary to this, a clearly lower I_D/I_G of 0.38 was obtained for $6VO_x/SiO_2$-P, indicating the highest graphitization extent of coke species.[7,16,56] As revealed from the analyses of the by-product selectivity, the $6VO_x/SiO_2$-P catalyst with dominated V_2O_5 is the most favorable to break C–C bond *via* the CO_2-RP and cracking reactions, while the remaining catalysts are more promising for CO_2-ODP. Thus, the highest graphitization extent of coke species over $6VO_x/SiO_2$-P may originate from the side reactions, which is favorable to form the coke species with a higher graphitization extent. This is consistent with previous work.[57] Additionally, the coke content decreased in the order of $6VO_x$–SiO_2-H > $4VO_x$–SiO_2-H > $6VO_x/SiO_2$-I > $6VO_x/SiO_2$-P, which coincides well with their propane conversion (Fig. 2a), meaning that the catalyst which converts more propane shows a higher content of coke. Following this understanding, the apparent coking rate, which is defined as the amount of the coke by converting 1 mol propane (g mol^{-1}) over the catalyst for CO_2-ODP was calculated. As given in Table 3, the coking rate was determined as 0.45 ± 0.03 g mol^{-1} for $4VO_x$–SiO_2-H, $6VO_x$–SiO_2-H and $6VO_x/SiO_2$-I, indicating a similar coke deposition behavior on the surface of catalysts. On the contrary, the significantly higher coking rate of 1.05 g mol^{-1} was obtained for $6VO_x/SiO_2$-P, which coincides well with the highest graphitization extent of coke species (Table 3). It is worth noting that if the relative deactivation rate of the catalysts ($R_{propane}$, Fig. 2d) was compared with either the coke content or the coking rate (Table 3), no obvious correlation of the catalytic stability with the deposited coke can be found, suggesting that the coke deposition may be not the critical factor in determining the stability of the catalysts.

Table 3 Coke deposition analysis and V oxidation state distribution over the spent catalysts for CO_2-ODP after a TOS of 128 min

Catalyst	Coke content[a] (wt%)	I_D/I_G[b]	Coking rate[c] (g mol^{-1})	V oxidation state distribution[d] (%)		
				V^{5+}	V^{4+}	V^{3+}
$4VO_x$–SiO_2-H	0.87	0.82	0.49	69.4	30.6	0
$6VO_x$–SiO_2-H	0.91	0.74	0.50	61.8	31.1	7.1
$6VO_x/SiO_2$-I	0.58	0.66	0.47	51.5	27.0	21.5
$6VO_x/SiO_2$-P	0.41	0.38	1.06	25.1	29.1	45.8

[a] Determined by the TG results as given in Fig. S9 (ESI). [b] Calculated based on the visible Raman results as given in Fig. S10 (ESI). [c] Calculated based on the amount of the coke by converting 1 mol propane. [d] Determined by the XP spectra results as given in Fig. 5b.

According to the redox mechanism of CO_2-ODP, the ability to replenish the active oxygen species by CO_2 to complete the redox cycles of VO_x plays an important role in determining the stability of the catalysts. To confirm this viewpoint, the relative deactivation rate ($R_{propane}$) was correlated with the amount of released CO per gram of V over the catalyst. As shown in Fig. 5a, an almost linear relationship was obtained, *i.e.*, a higher amount of released CO, a lower $R_{propane}$. This indicates that the catalyst shows a better stability provided that the reduced VO_x species over the catalyst is more easily re-oxidized by CO_2. As a result, the best stability was obtained over the $4VO_x$–SiO_2-H catalyst with dominantly monomeric VO_x species. Taking the structural and chemical properties of different VO_x species into account, the V^{5+} species with a higher polymerization extent or domain size over the parent catalysts was more easily reduced to V^{3+} (Table 2), which cannot be effectively re-oxidized by CO_2 to V^{5+} to complete the redox cycles.[18,54] Thus, the deep reduction of V^{5+} to V^{3+} during the reaction may be associated with the catalyst deactivation. To confirm this, the spent catalysts after CO_2-ODP for a TOS of 128 min were characterized by XPS. As shown in Fig. 5b, the binding energy of V $2p_{3/2}$ over the spent catalysts shifted to a lower value in comparison with that of the fresh catalysts (517.6 eV, Fig. S4, ESI†), indicating an increased content of VO_x with a lower oxidation state[18,22] after the CO_2-ODP reaction. To make a quantitative comparison, the V $2p_{3/2}$ spectra were deconvoluted. As given in Fig. 5b, three peaks at 515.7, 516.6 and 517.6 eV assigned to V^{3+}, V^{4+} and V^{5+} species,[22,58] respectively, were observed. The relative fractions of V^{3+}, V^{4+} and V^{5+} over the spent catalysts were calculated by respective peak area. As shown in Table 3, the relative fraction of V^{5+} deceased from 69.4% to 25.1% in the order of $4VO_x$–SiO_2-H > $6VO_x$–SiO_2-H > $6VO_x/SiO_2$-I > $6VO_x/SiO_2$-P, the change pattern is consistent with that of their catalytic stability, *i.e.*, the higher content of V^{5+} remained on the spent catalyst surface, the better stability of the catalyst was (Fig. S11a, ESI†). Contrary to this, when the relative fraction of V^{3+} was correlated with the stability of the catalysts, an opposite order

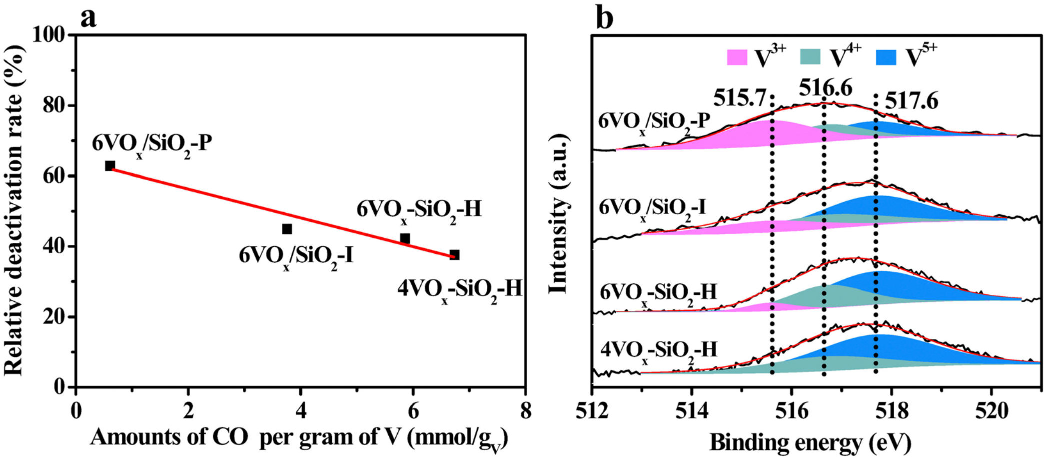

Fig. 5 Correlation of relative deactivation rate ($R_{propane}$) with the amount of formed CO per gram of V over the catalyst during CO_2 pulse experiments (a), and V $2p_{3/2}$ XP spectra of the spent catalysts after CO_2-ODP for a TOS of 128 min (b).

was found (Fig. S11b, ESI†). These results clearly indicate that the deep reduction of V^{5+} to V^{3+} is the key reason for the deactivation of the catalysts in CO_2-ODP. Thus, the redox rates of the VO_x species participated with CO_2 and propane are not very well matched, owning to the weak oxidizing ability of CO_2. This is consistent with the CO_2 pulse experiments and H_2-TPR results (Table 2).

Following the above discussion, the redox mechanism of CO_2-ODP catalyzed by the SiO_2-supported VO_x catalysts with isolated VO_x species is illustrated in Scheme 2. Propane reacts with the active oxygen of V^{5+} to produce propene and water, resulting in the formation of reduced VO_x with an oxidation state of +4. To complete the redox cycle, CO_2 reacts with the V^{4+} species to release CO and simultaneously replenish the active oxygen species. With increasing the polymerization extent or domain size of supported VO_x species, the matching of the redox cycles of VO_x during the CO_2-ODP reaction was hindered, due to the formation of deeply reduced VO_x species with a lower oxidation state of +3, which cannot be efficiently re-oxidized by CO_2 to V^{5+}. As a result of the highest dispersion of VO_x species over $4VO_x$–SiO_2-H, the best performance for CO_2-ODP was obtained among the evaluated catalysts.

4. Conclusions

In summary, four SiO_2-supported VO_x catalysts with narrow distributions of V loading while well-defined structures of VO_x species were synthesized by applying appropriate preparation methods. The dominated monomeric and less polymeric VO_x were formed over the $4VO_x$–SiO_2-H and $6VO_x$–SiO_2-H catalysts, respectively, prepared by one-pot hydrothermal synthesis. In case of the $6VO_x/SiO_2$-I catalyst prepared by simply impregnation method, the highly polymerized VO_x with a small amount of V_2O_5 was present, while V_2O_5 crystallites were overwhelmingly predominant over the $6VO_x/SiO_2$-P catalyst prepared by physic grinding method. The catalytic activity and stability for CO_2-ODP decreased in the order of $4VO_x$–SiO_2-H > $6VO_x$–SiO_2-H > $6VO_x/SiO_2$-I > $6VO_x/SiO_2$-P, which can be explained

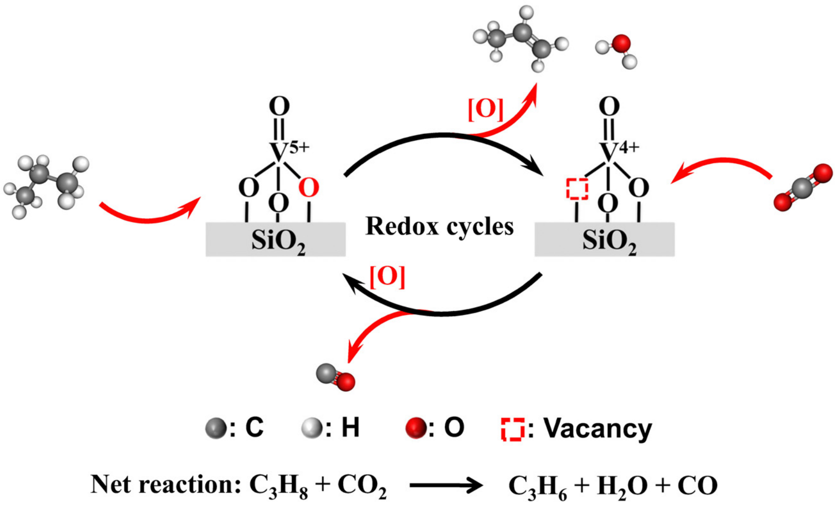

Scheme 2 Redox mechanism over supported VO_x catalyst for CO_2-ODP.

by the ability for re-oxidation of the reduced VO_x species with different structures by CO_2. The reduced monomeric VO_x is the most easily re-oxidized by CO_2, and thus the reduction/oxidation cycles of V^{4+}/V^{5+} species during the CO_2-ODP reaction can be well completed, leading to the best performance. With increasing the polymerization extent or domain size of supported VO_x species, the matching of the redox cycles of VO_x during the reaction was hindered, due to the formation of deeply reduced VO_x species with a lower oxidation state of +3, which cannot be efficiently re-oxidized by CO_2. These understandings can provide important contributions to the essential reason of the structural impacts of VO_x species on CO_2-ODP, which are beneficial to promote the development of highly active and stable VO_x-based catalysts for CO_2-ODP.

Author contributions

Li Wang: investigation, formal analysis, data curation, visualization, writing – original draft; Heng-Bo Zhang: conceptualization, investigation, formal analysis, data curation; Rong-Rong Hu and Han-Qing Ge: project administration; Guo-Qing Yang: conceptualization, investigation, methodology, writing – review & editing; Yuefeng Li, and Zhao-Tie Liu: investigation; Zhong-Wen Liu: conceptualization, supervision, writing – review & editing.

Data availability

The authors confirm that the data supporting the findings of this study are available within the article and its ESI.†

Conflicts of interest

There are no conflicts to declare.

Acknowledgements

This work was supported by the National Natural Science Foundation of China (grant number 22338010).

References

1 S. Chen, X. Chang, G. Sun, T. Zhang, Y. Xu, Y. Wang, C. Pei and J. Gong, *Chem. Soc. Rev.*, 2021, **50**, 3315–3354.
2 T. Otroshchenko, G. Jiang, V. A. Kondratenko, U. Rodemerck and E. V. Kondratenko, *Chem. Soc. Rev.*, 2021, **50**, 473–527.
3 X. Jiang, L. Sharma, V. Fung, S. J. Park, C. W. Jones, B. G. Sumpter, J. Baltrusaitis and Z. Wu, *ACS Catal.*, 2021, **11**, 2182–2234.
4 Y. Yuan, W. N. Porter and J. G. Chen, *Trends Chem.*, 2023, **5**, 840–852.
5 H. Guo, Z. Xie, X. Wang, J. G. Chen and P. Liu, *EES Catal.*, 2023, **1**, 17–25.
6 E. Gomez, B. Yan, S. Kattel and J. G. Chen, *Nat. Rev. Chem.*, 2019, **3**, 638–649.
7 J. Wang, Y.-H. Song, Z.-T. Liu and Z.-W. Liu, *Appl. Catal., B*, 2021, **297**, 120400.
8 S. Zhang, C.-a Zhou, S. Wang, Z. Qin, G. Shu, C. Wang, L. Song, L. Zheng, X. Wei, K. Ma and H. Yue, *Chem. Eng. J.*, 2024, **481**, 148231.
9 M. Chen, J. Xu, Y. Cao, H.-Y. He, K.-N. Fan and J.-H. Zhuang, *J. Catal.*, 2010, **272**, 101–108.
10 H. Xiao, J. Zhang, P. Wang, X. Wang, F. Pang, Z. Zhang and Y. Tan, *Catal. Sci. Technol.*, 2016, **6**, 5183.
11 G.-Q. Yang, Y.-J. He, Y.-H. Song, J. Wang, Z.-T. Liu and Z.-W. Liu, *Ind. Eng. Chem. Res.*, 2021, **60**, 17850–17861.
12 E. Nowicka, C. Reece, S. M. Althahban, K. M. H. Mohammed, S. A. Kondrat, D. J. Morgan, Q. He, D. J. Willock, S. Golunski, C. J. Kiely and G. J. Hutchings, *ACS Catal.*, 2018, **8**, 3454–3468.
13 G.-Q. Yang, X. Ren, V. A. Kondratenko, H.-B. Zhang, E. V. Kondratenko and Z.-W. Liu, *Nano Res.*, 2023, **16**, 6237–6250.
14 F. Xing, Y. Nakaya, S. Yasumura, K.-I. Shimizu and S. Furukawa, *Nat. Catal.*, 2022, **5**, 55–65.
15 K.-X. Li, X. Cai, H.-B. Liu, X.-Y. Liu, Y. Shan, X. Feng and D. Chen, *React. Chem. Eng.*, 2024, **9**, 1292–1312.
16 X. L. Xue, W. Z. Lang, X. Yan and Y. J. Guo, *ACS Appl. Mater. Interfaces*, 2017, **9**, 15408–15423.
17 Y.-L. Shan, H.-L. Sun, S.-L. Zhao, P.-L. Tang, W.-T. Zhao, J.-W. Ding, W.-L. Yu, L.-N. Li, X. Feng and D. Chen, *ACS Catal.*, 2022, **12**, 5736–5749.
18 G.-Q. Yang, H. Wang, T. Gong, Y.-H. Song, H. Feng, H.-Q. Ge, H.-B. Ge, Z.-T. Liu and Z.-W. Liu, *J. Catal.*, 2019, **380**, 195–203.
19 J. Wang, M.-L. Zhu, Y.-H. Song, Z.-T. Liu, L. Wang and Z.-W. Liu, *J. Catal.*, 2022, **409**, 87–97.
20 I. Takahara, M. Saito, M. Inaba and K. Murata, *Catal. Lett.*, 2005, **102**, 201–205.
21 H. Wang, W. Zhu, G.-Q. Yang, Y.-W. Zhang, Y.-H. Song, N. Jiang, Z.-T. Liu and Z.-W. Liu, *Ind. Eng. Chem. Res.*, 2019, **58**, 21372–21381.
22 G. Liu, Z.-J. Zhao, T. Wu, L. Zeng and J. Gong, *ACS Catal.*, 2016, **6**, 5207–5214.
23 Z. Wu, H.-S. Kim, P. C. Stair, S. Rugmini and S. D. Jackson, *J. Phys. Chem. B*, 2005, **109**, 2793–2800.
24 U. Rodemerck, M. Stoyanova, E. V. Kondratenko and D. Linke, *J. Catal.*, 2017, **352**, 256–263.
25 K. Chen, A. T. Bell and E. Iglesia, *J. Catal.*, 2002, **209**, 35–42.
26 H. Tian, E. I. Ross and I. E. Wachs, *J. Phys. Chem. B*, 2006, **110**, 9593–9600.
27 O. Schwarz, D. Habel, O. Ovsitser, E. V. Kondratenko, C. Hess, R. Schomäcker and H. Schubert, *J. Mol. Catal. A: Chem.*, 2008, **293**, 45–52.
28 C. A. Carrero, R. Schloegl, I. E. Wachs and R. Schomaecker, *ACS Catal.*, 2014, **4**, 3357–3380.
29 Z.-F. Han, X.-L. Xue, J.-M. Wu, W.-Z. Lang and Y.-J. Guo, *Chin. J. Catal.*, 2018, **39**, 1099–1109.
30 W. Wang, S. Chen, C. Pei, R. Luo, J. Sun, H. Song, G. Sun, X. Wang, Z.-J. Zhao and J. Gong, *Science*, 2023, **381**, 886–890.

31 Q. Liu, J. Li, Z. Zhao, M. Gao, L. Kong, J. Liu and Y. Wei, *Catal. Sci. Technol.*, 2016, **6**, 5927–5941.
32 H. Xiao, J. Zhang, P. Wang, X. Wang, F. Pang, Z. Zhang and Y. Tan, *Catal. Sci. Technol.*, 2016, **6**, 5183–5195.
33 J. Wang, L. Liu, J. Feng, X. Zhang, X. Ju and P. Chen, *Catal. Sci. Technol.*, 2022, **12**, 5339–5348.
34 M. Numan, E. Eom, A. Li, M. Mazur, H. W. Cha, H. C. Ham, C. Jo and S.-E. Park, *ACS Catal.*, 2021, **11**, 9221–9232.
35 R. J. Madon and M. Boudart, *Ind. Eng. Chem. Fundam.*, 1982, **21**, 438–447.
36 M. Zhang, M. Wang, B. Xu and D. Ma, *Joule*, 2019, **3**, 2876–2883.
37 Q.-X. Luo, X.-K. Zhang, B.-L. Hou, J.-G. Chen, C. Zhu, Z.-W. Liu, Z.-T. Liu and J. Lu, *Catal. Sci. Technol.*, 2018, **8**, 4864–4876.
38 Z. Wu, S. Dai and S. H. Overbury, *J. Phys. Chem. C*, 2010, **114**, 412–422.
39 J. T. Grant, C. A. Carrero, A. M. Love, R. Verel and I. Hermans, *ACS Catal.*, 2015, **5**, 5787–5793.
40 X. Gao, S. R. Bare, B. M. Weckhuysen and I. E. B. Wachs, *J. Phys. Chem. C*, 1998, **102**, 10842–10852.
41 G. T.-M. Christian Hess and R. Herbert, *J. Phys. Chem. C*, 2007, **111**, 9471–9479.
42 X. Gao, J.-M. Jehng and I. E. Wachs, *J. Catal.*, 2002, **209**, 43–50.
43 M. D. Argyle, K. Chen, C. Resini, C. Krebs, A. T. Bell and E. Iglesia, *J. Phys. Chem. B*, 2004, **108**, 2345–2353.
44 S. Dzwigaj, M. Matsuoka, M. Anpo and M. Che, *J. Phys. Chem. B*, 2000, **104**, 6012–6020.
45 H. Zhang, S. Cao, Y. Zou, Y.-M. Wang, X. Zhou, Y. Shen and X. Zheng, *Catal. Commun.*, 2014, **45**, 158–161.
46 X. Gao and I. E. Wachs, *J. Phys. Chem. B*, 2000, **104**, 1261–1268.
47 Y. Liu, W. Feng, T. Li, H. He, W. Dai, W. Huang, Y. Cao and K. Fan, *J. Catal.*, 2006, **239**, 125–136.
48 G.-Q. Yang, Y. Niu, V. A. Kondratenko, X. Yi, C. Liu, B. Zhang, E. V. Kondratenko and Z.-W. Liu, *Angew. Chem., Int. Ed.*, 2023, **62**, e202310062.
49 Y.-M. Liu, Y. Cao, N. Yi, W.-L. Feng, W.-L. Dai, S.-R. Yan, H.-Y. He and K.-N. Fan, *J. Catal.*, 2004, **224**, 417–428.
50 M. M. Koranne, J. G. Goodwin and G. Marcelin, *J. Catal.*, 1994, **148**, 369–377.
51 S. Chen, C. Pei, X. Chang, Z.-J. Zhao, R. Mu, Y. Xu and J. Gong, *Angew. Chem., Int. Ed.*, 2020, **59**, 22072–22079.
52 F. Xing and S. Furukawa, *Chem. – Eur. J.*, 2023, **29**, e202202173.
53 I. Ascoop, V. V. Galvita, K. Alexopoulos, M.-F. Reyniers, P. Van Der Voort, V. Bliznuk and G. B. Marin, *J. Catal.*, 2016, **335**, 1–10.
54 M.-S. Park, V. P. Vislovskiy, J.-S. Chang, Y.-G. Shul, J. S. Yoo and S.-E. Park, *Catal. Today*, 2003, **87**, 205–212.
55 Z. W. Liu, C. Wang, W. B. Fan, Z. T. Liu, Q. Q. Hao, X. Long, J. Lu, J. G. Wang, Z. F. Qin and D. S. Su, *ChemSusChem*, 2011, **4**, 341–345.
56 H. Wang, G.-Q. Yang, Y.-H. Song, Z.-T. Liu and Z.-W. Liu, *Catal. Today*, 2019, **324**, 39–48.
57 L. Wang, G.-Q. Yang, X. Ren and Z.-W. Liu, *Nanomaterials*, 2022, **12**, 417.
58 S. Chen, L. Zeng, R. Mu, C. Xiong, Z.-J. Zhao, C. Zhao, C. Pei, L. Peng, J. Luo, L.-S. Fan and J. Gong, *J. Am. Chem. Soc.*, 2019, **141**, 18653–18657.